Electronic Supplementary Material (ESI) for Nanoscale Advances.

Supporting information

pH-Regulated Thermo-driven Nanofluidics for Nanoconfined Mass Transport and Energy Conversion

Xiaolu Zhao [#a,b,c], *Long Li* [#b], *Wenyuan Xie* [b], *Yongchao Qian* [a,c], *Weipeng Chen* [a,c], *Bo Niu* [a,c], *Jianjun Chen* [a,c], *Xiang-yu Kong* [a], *Lei Jiang* [a, c], *Liping Wen* *[a,c]

a. CAS Key Laboratory of Bio-inspired Materials and Interfacial Science, Technical Institute of Physics and Chemistry, Chinese Academy of Sciences, Beijing 100190, PR China.

b. Qian Xuesen Laboratory of Space Technology, Beijing 100049, PR China.

c. University of Chinese Academy of Sciences, Beijing 100049, PR China.

1. Experimental procedures

Nanochannel Fabrication

The porous PI membrane (12 μm) was firstly prepared by mature ion track etching technique. The membrane was firstly irradiated by swift heavy ions (Au) of energy 11.4 MeV per nucleon. And then it was exposed under the UV irradiation for 1.5 hours of each side. Two chambers of conductivity cell were used as etching instruction where the membrane was fixed between two of them. One was immersed with 1 mol L^{-1} KI while the other was filled with NaClO aqueous solution (17% wt). A voltage (1 V) was exerted by a pair of Pt electrodes to establish the current across the membrane. The stopping process was acted immediately once it has been achieved the desired current.

Chemical Modification

PI membrane was floated on a solution (3 mL) consisting of DOPA (6 mg) and Tris HCl bu□er (3 mL, pH=8.5) for 6h. The functional molecule DOPA modified the PI membrane from the base side and reacted with the inner surface of the conical-shaped nanochannel by capillary effect. After modification, the membrane was washed with deionized water repeatedly.

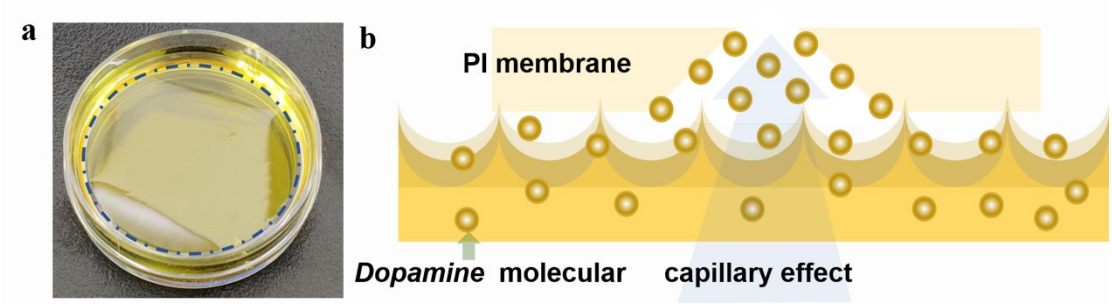

Figure S1. The asymmetric modification method. (a) schematic illustration of capillary effect, (b) picture of membrane floating on the DOPA solution.

***I-V* curves measurement**

These measurements were performed recorded using a Keithley 6430 picoammeter (Keithley Instruments, Cleveland, OH). The membrane was fixed between the two costumed cells, which was similar with that applied for etching process. A pair of Ag/AgCl electrodes was used.

Thermometric conversion capability

It was recorded by a similar homemade system. A pair of Ag/AgCl sheet electrodes was immersed into the aqueous solution and two groups of thermocouples (Type K calibration, Omega Engineering Inc.) were mounted inner the cell symmetrically and connected to a data acquisition device (DAQ, NI9203) to collect the temperature variations. The thermocouples were fixed near the membrane as soon as possible. The I-V curves were tested for 5 times at variable temperature gradient. The low temperature was set at 20℃. The electrolyte was 0.1 mol L^{-1} with normal pH (6.5). The direction where the base side was set near hot source was named of forward direction, and the opposite was named of reverse direction. Other details were listed in Section S7.

Materials and Characterization

Polyimide (PI, 12 μm thick) (GSI, Darmatadt, Germany). Sodium hypochlorite (NaClO), potassium iodide (KI), dopamine and potassium chloride (KCl) were purchased from Shanghai Aladdin Biochemical Technology Co., Ltd. SEM images were taken in the field-emission mode using Hitachi S-4800 at an accelerating voltage of 10 kV. UV-visible absorption spectra were recorded by UV-3600 spectrometer (Shimadzu, Japan). Zeta measurements were acted through planar membrane modified by PDOPA.

2. Geometrical features of the conical nanochannel

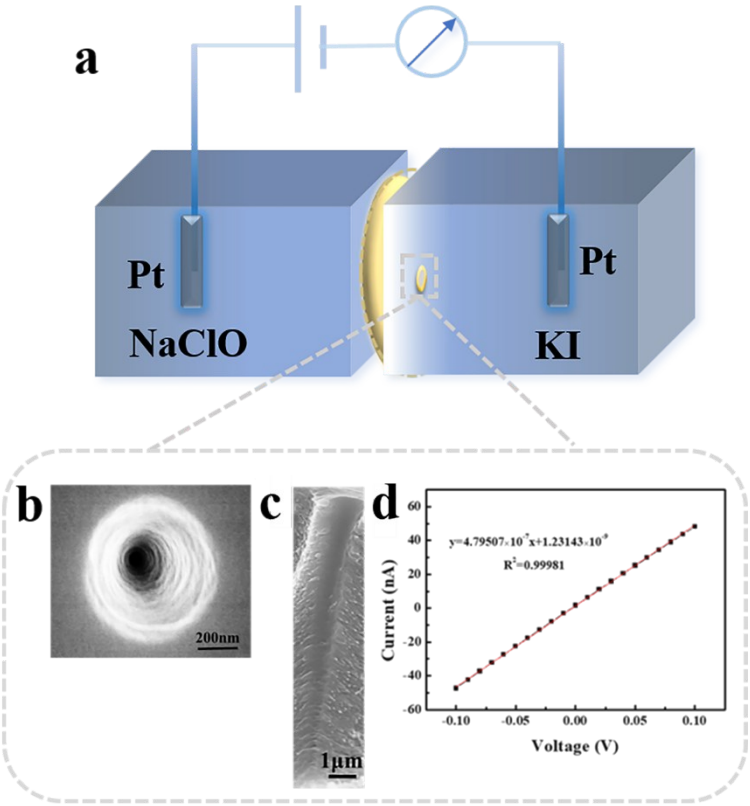

Figure S2 Chemical etching and geometrical features of the conical nanochannel. (a) the scheme of chemical etching process, (b) the SEM image of base side, (c) the cross-section view, (d) *I*-*V* curves from -0.1 V to 0.1 V tested for 10 times.

Two chambers of conductivity cell were used as etching instruction where the membrane was fixed between two of them. The diameter of base side in a conical nanochannel was about 750 nm observed from SEM images (Figure S1 a, b). The diameter of tip side was calculated by following equation[1].

$$d_{tip} = \frac{4LI}{\pi k(c)UD}$$

Herein, L is the length of pore (12 μm), I and U is the current and voltage, respectively. k(c) is the conductivity of the electrolyte. For 1mol/L KCL aqueous solution at 25 ℃, k(c) is equal to 0.11173 S/cm. In this paper, the tip diameter was about 180 nm.

3. Illustrations of the fabrication of PI membrane modified by dopamine

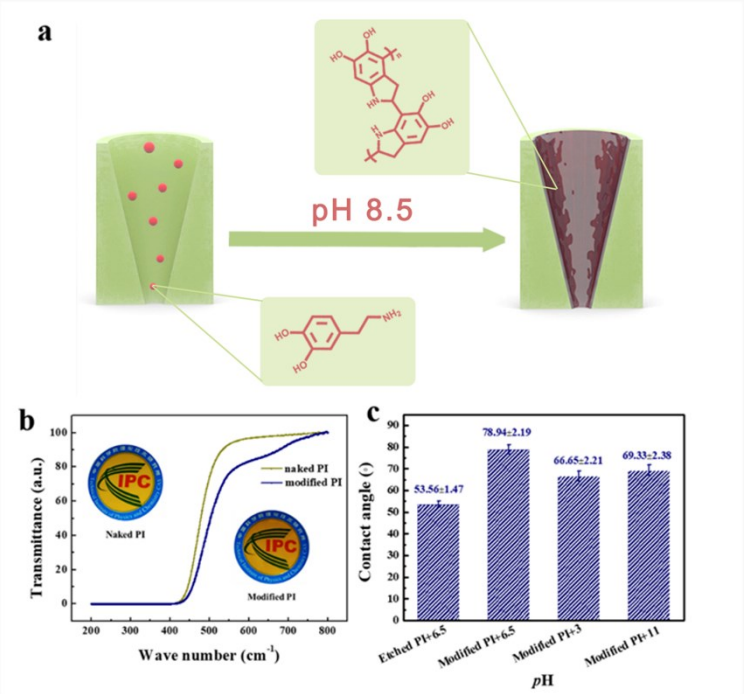

Figure S3 Illustrations of the fabrication of PI membrane modified by dopamine. (a)the fabrication of hybrid membrane with abundant functional groups including the chemical equation of self-polymerization of dopamine, (b) the transmittance of naked and modified PI membrane scanning from 200 to 800 cm^{-1}, the inset is the photos of naked and modified PI membrane, (c) contact angle of etched PI membrane and modified one of the contacted side between DOPA solution and membrane. The membranes were immersed into corresponding solvents for 2 hours in advance.

PI membrane was exerted to float onto DOPA aqueous solution, which enabled the ingrained bonding and uniform integration.

4. *I-V* curves of naked and modified PI membrane

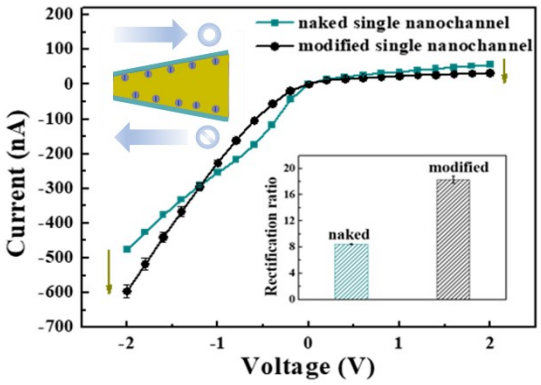

Figure S4 *I-V* curves of naked and modified PI membrane at 0.1 mol/L KCl aqueous solution at normal pH conditions scanning from -2 to 2 V for 10 times. The rectification ratio was calculated using the absolute value of current at -2 V to divide that of current at 2 V (in the inset).

5. Washburn model [2]

$$x = \sqrt{\frac{\gamma h cos\theta}{3\mu}t}$$

Herein, the moving length (x) is a function of time (t), where μ is the viscosity of the liquid, γ is the surface tension of the liquid in air, h is the channel height and θ is the contact angle[1]. Considering the complex variation of h and θ inner the surface of conical nanochannel, we calculated a wide range of velocity due to alternate diameter along the axis. Obtained from the chemical handbook, the surface tension and viscosity of 0.1 mol/L KCl aqueous solution is 72.79 mN/m, 1 mPa/s, the contact angle was replaced by static contact angle (Figure S2c). The x is approximately equal to 12 μm. The channel height can be defined by alternate diameter along the axis from 750 nm to 180 nm. Based on corresponding parameters, the velocity changed from 0.00164 m/s to 0.00091 m/s. Therefore, the longest time is merely about 0.013s theoretically. Considering exceptional processability and excellent reproducibility, PI membrane was exerted to float onto DOPA aqueous solution, which enabled the ingrained bonding and uniform integration. The tip of that is modified in small quantities due to capillary effect. Although the reduced experimental flow speed compared to the model has been widely observed due to strong wall-liquid interaction and the difference of contact angle between planar and curved section, the deliberate prolong time (6h) can ensure advantageous modification of DOPA proved by dual improvement between ion selectivity and ionic flux. In tandem with efficient unilateral side contact, complete immersion increases the risks of non-uniform or over-modification, possibly resulting in the reduced ionic flux and selectivity.

6. Thickness of double electric layer[2]

$$\lambda = \sqrt{\varepsilon k_b \varepsilon_0 T / 2 n_{bulk} z^2 e^2}$$

Where:

λ is the thickness of double electric layer

ε is the relatively dielectric constant

ε_0 is the dielectric constant of vacuum

k_b is Boltzmann constant

n_{bulk} is the concentration of bulk phase

z is the charge electron

e is the electricity of single electron

7. Experimental set-up of thermoelectric conversion device

The capability of power generation was examined with a customized device, where the base side of single nanochannel varied technically toward cold side or hot side as required and 0.1 mol/L KCl electrolyte was used on both sides. A pair of Ag/AgCl electrodes was applied to measure streaming current. The membrane was mounted tightly between the two tetrafluoroethylene cells. If necessary, the tetrafluoroethylene cell was replaced by alumina cell. The thermal probe was insulated and was stick in the cells. They were immersed into the solution and their height is near the nanochannel region. the accuracy is ±0.1 K The refreshing frequency is 1 s^{-1}. The streaming current was estimated by picoammeter. The heating plate was glued at the bottom of alumina cell to maintain the high temperature and the condensate water is through the tetrafluoroethylene to decrease the heat transfer. At the beginning of experiment, the setup needs calibration in order to keep horizontal. The maintain time of temperature difference is relatively short, thus the condition of constant temperature is adopted at measurement of *I-V* curve experiments.

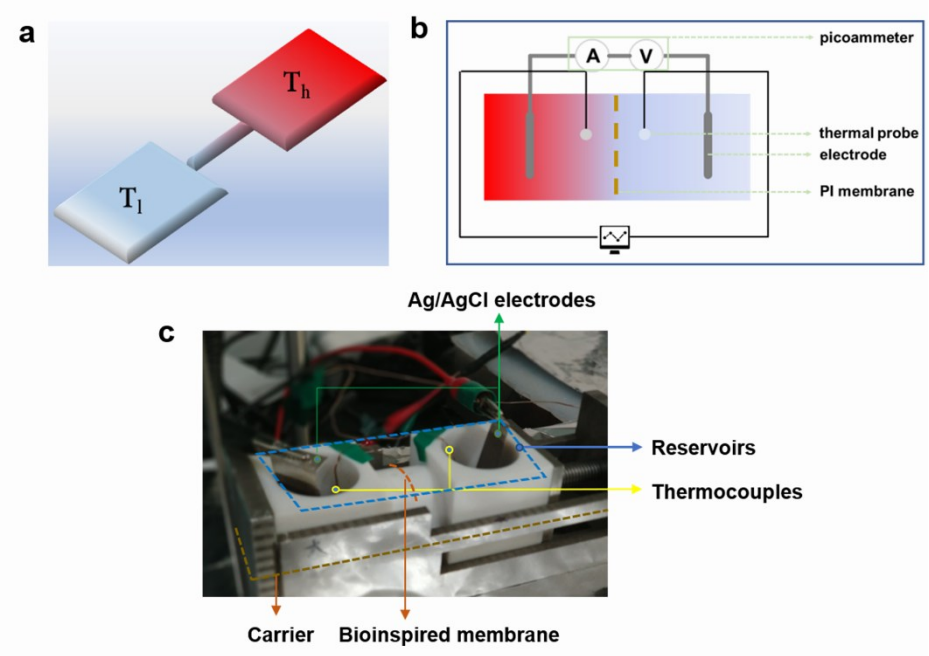

Figure S5 A custom device of examining thermoelectric generation capability. (a) schematic illustration of the custom device, the base side can be tuned as required towards hot sources or cold sources, (b) the setup of electrode and thermal probe, (c) Photo of the nanofluidic system.

8. Alignment of device

In all cases, the anode was set near the base side while the device was aligned to horizontal position in advance.

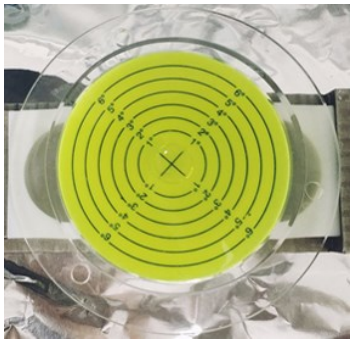

Figure S6 Photo of device with horiztional axis after alignment with the help of a spirit level.

9. Schematic illustration of thermo-driven ion transport

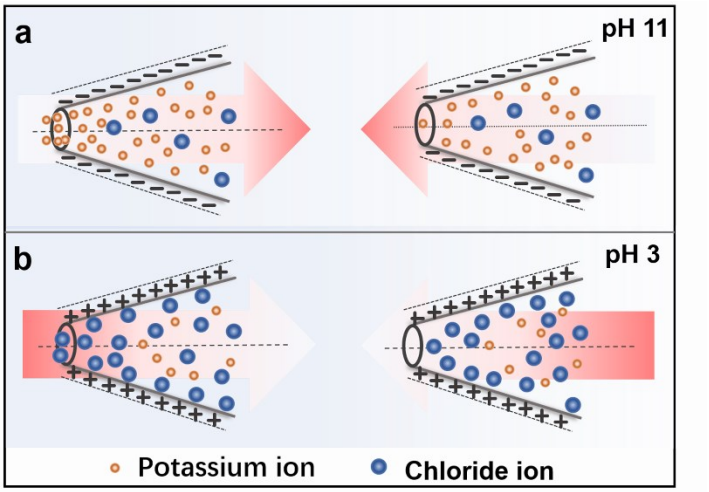

Figure S7. Ion transport with pH modulation driven by low-grade heat. (a) at alkaline condition, the cations were transported from tip to base side preferentially, (b) while at acid condition, the cations were transported from base to tip side preferentially.

10. Numerical simulation

Numerical simulation of directed flow was based on the finite-element software package COMSOL Multiphysics (version 5.4). We coupled Poisson-Nernst-Planck equation (PNP), Naiver-Stokes equation (NS) and complex energy equation (heat transfer) to describe the basic parameters of nanochannel, discussed their liable effect for mass transport and liquid in nanoconfined geometry flow under the temperature gradient. Advection, viscous dissipation, and joule heating could be neglected in the energy equation[3-5]. The total length was 2 μm, the diameter of tip side was 20nm and the base side was 400nm. The concentration of electrolyte was constantly 0.1 mol/L KCl regardless of *p*H. For heat transfer module, two electrolyte reservoirs were set to different temperature conditions while other walls were considered to be insulated ($-n\cdot q=0$, where n was the unit outer normal vector of the wall and q was the wall heat flux).

Poisson-Nernst-Planck equation (PNP):

$$J_i = D_i\left(\nabla c_i + \frac{z_i F c_i}{RT}\nabla\varphi\right) + c_i u$$

$$\nabla^2\varphi = -\frac{F}{\varepsilon}\sum z_i c_i$$

$$\nabla\bullet J_i = 0$$

Naiver-Stokes equation (NS) and continuity equation:

$$\rho\left(\frac{\partial u}{\partial t} + (u_c\cdot\nabla)u\right) = \nabla\cdot[-pI + \mu(\nabla u + (\nabla u)^T)]$$

$$\nabla\cdot u = 0$$

The bulk ion concentration at the reservoirs was 0.1M. The ion-impenetrable condition was applied at the nanochannel wall ($n\cdot J_i = 0$). The surface charge density ($\sigma = -\varepsilon_0\varepsilon_r n\cdot\nabla\varphi$) was set at the channel wall and was calculated by Grahame equation. The base side was set to ground (voltage $V = 0\ mV$) and the surface charge density at the remaining wall was zero.

Energy equation:

$$\rho C_p\left(\frac{\partial T}{\partial t}+(u_c\cdot\nabla)T\right)=\nabla\cdot(k\nabla T)$$

In general, considering the channel size, the continuity model is still effective and the relevant control equations and boundary conditions can be safely applied[6]. Simultaneously the physical properties of the working medium can be simply set and remain constant during the iteration of the computational process. We have systematically evaluated the numerical method and implemented detailed information on the assessment of the simulation accuracy. Mesh independence has been verified as suggested, which represents both good stability and accuracy of the numerical solution (Figure S8). From the simulation results, the voltage of tip side for 108564 and 211981 elements are nearly constant. Hence, the number of elements used in subsequent simulations is set to108564 in order to balance the calculation speed and accuracy of the model. To further validate the numerical method, benchmark solutions of the PNP equations in the cylindrical geometry have been solved and compared with the approximate analytical (PL) solution derived by Petsev and Lopez[7].

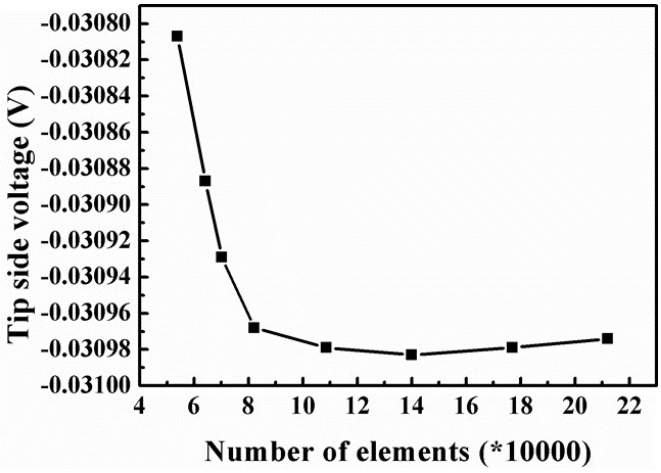

Figure S8 Grid independence test.

From the simulation results, the voltage of tip side for 108564 and 211981 elements are nearly constant. Hence, the number of elements used in subsequent simulations is set to108564 in order to balance the calculation speed and accuracy of the model.

Where:

$\boldsymbol{J}_i$, D_i, c_i, φ, $\boldsymbol{u}$, R, F, T, z_i, ε is the ion flux, diffusion coefficient, ion concentration,

electrical potential, fluid velocity, universal gas constant, Faraday constant, absolute temperature, valence and dielectric constant of the electrolyte solutions, respectively. ρ, p, C_p, μ is the density, pressure, heat capacity, kinetic viscosity.

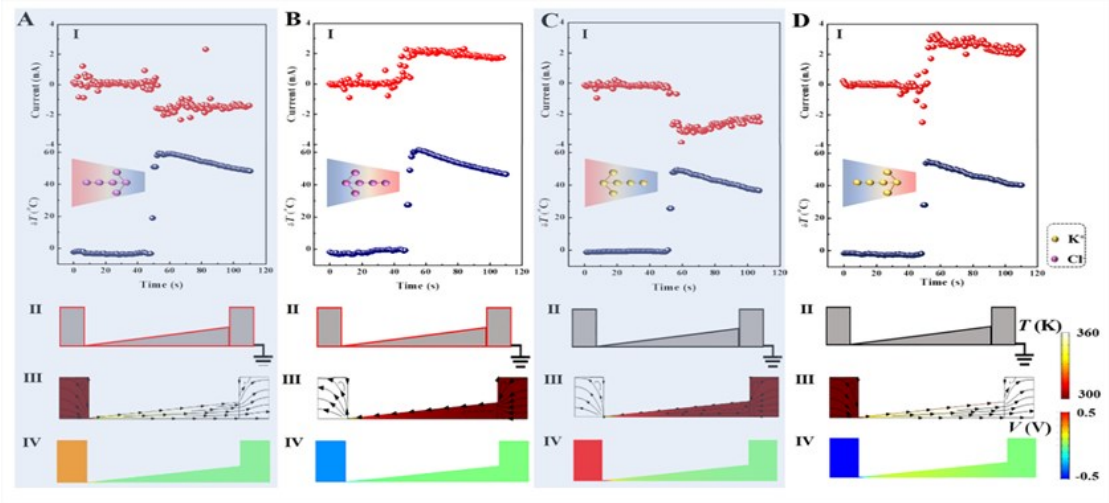

Figure S9 Streaming current obtained by thermal energy. Ⅰ Copy from Figure 2. Ⅱ Numeric simulation model: (A), (B) The surface was governed by positive charge; (C), (D) The surface was governed by negative charge. The based side was set to the ground. Ⅲ Simulative velocity of nanofluidics driven by temperature difference. Ⅳ Numeric simulation of thermoelectric voltage. At pH=3, surplus Cl^- ions diffused from hot to cold source thus the voltage of tip side was higher. At pH=11, surplus K^+ ions diffused from cold to hot source thus the voltage of base side was higher.

11. Grahame equation and Laminar flow module

$$\sigma = \sqrt{8\epsilon kT\varepsilon_0 c_0}\sinh(\frac{e\xi}{2kT})$$

Herein, c_0, k, T, ε, ε0, e is the concentration of the electrolyte, the Boltzmann constant, the absolute temperature (298 K), the dielectric constant of water (78.4 at T = 298 K), the permittivity of vacuum and the elementary charge, respectively.

Generally, by neglecting the potential decrease occurring in the Stern layer and any contribution of specific ion adsorption, the zeta potential can be assumed to be equal to surface potential. The zeta potential can be obtained from the practical measurements (Figure 1c). Thus, the surface charge density can be calculated from the surface potential of the membrane at respective pH conditions by Grahame equation.

Laminar flow module: The slip velocity condition was applied at the channel wall combining the viscous slip and thermo-osmotic flow:

$$v_s = \frac{L_s}{\mu}\tau - \frac{\sigma_T \mu}{\rho T}\nabla T$$

Where:

L_s and τ are the slip length and the shear stress at the wall, respectively. μ is the dynamic viscosity and σ_T is the thermal-slip coefficient. No-slip condition was set at the remaining wall and the pressure of two reservoirs was 1 atm. It was observed that thermal-slip coefficient had a great effect on slip velocity.

12. Ion distribution inner the nanochannel

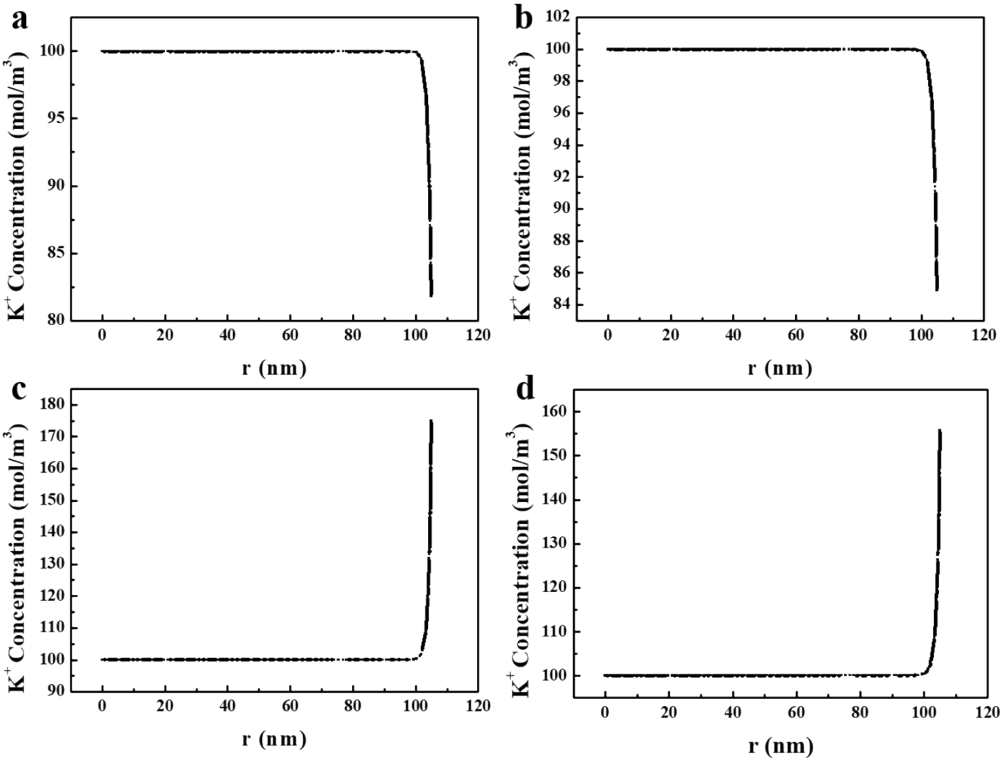

Figure S10 ion distribution inner the nanochannel. At pH =3, (a) the base side was set toward hot source, (b) the base side was set toward cold source.; At pH =11, (c) the base side was set toward hot source, (d) the base side was set toward cold source.

13. Outpower generation at strongly alkali environment

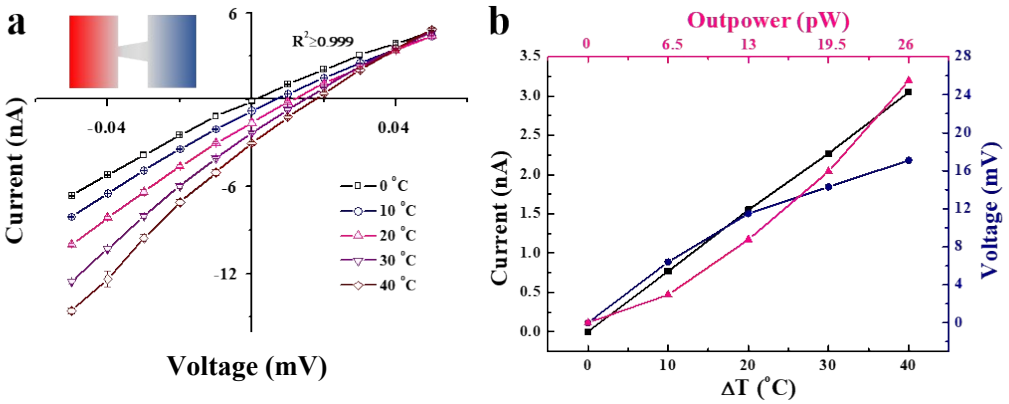

Figure S11 Outpower generation of forward direction under strongly alkali environment.

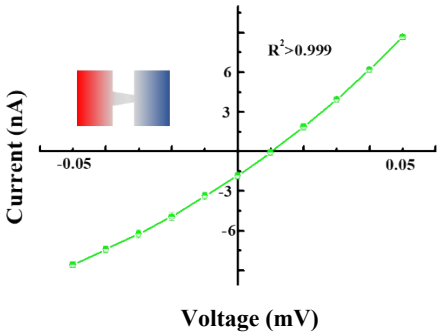

Figure S12 Outpower generation of reverse direction under strongly alkali environment at δT=40℃.

14. The comparison of recent advances

Table S1 Comparison of recent advances

Materials	Pore geometry (nm)	Concentration (M)	Open-circuit voltage (mV)	Thermopower (mV/℃)	Ref.
polyimide	11.27 conical	1	14.4 ΔT=40℃	0.36	[8]
SiO_2/PET	2.3/10~15 cylindrical	0.001	7.1 ΔT=10℃	0.71	[9]
$K_3[Fe(CN)_6]/K_4[Fe(CN)_6]$ poly (sodium acrylate)	50 nm 3D gel	0.1	27.25 ΔT=25℃	1.09	[10]
$Fe(CN)_6^{4-}$/ $Fe(CN)_6^{3-}$ poly (vinyl alcohol)	-- 3D gel	0.1	~24 ΔT=20℃	1.21	[11]
$FeCl_2/FeCl_3$ poly (vinyl alcohol)	-- 3D gel	0.1	~20 ΔT=20℃	1.02	[11]
$Fe(CN)_6^{4-}$/ $Fe(CN)_6^{3-}$ polyacrylamide	3D gel	0.1	~24 ΔT=20℃	1.2	[12]
DOPA-PI	<180 conical	0.1	~8 ΔT=10℃	0.8	☆

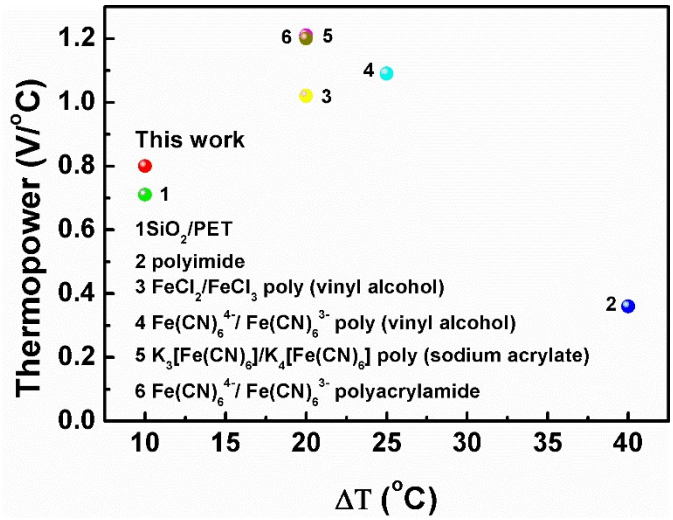

Figure 13 Comparison of recent advances for thermopower.

15. Tunable thermoelectric conversion with the period of 100~120s

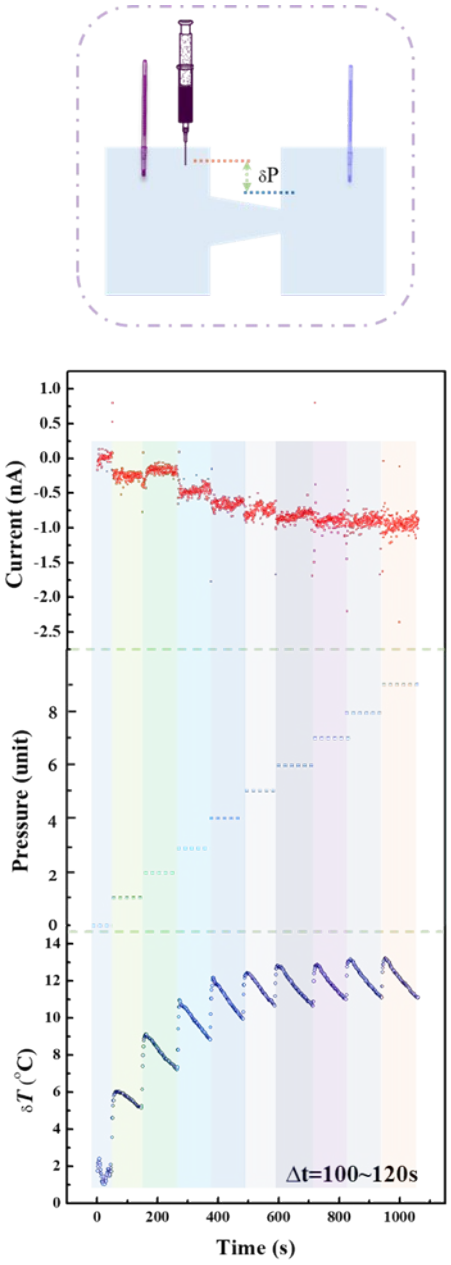

Figure S14 Tunable thermoelectric conversion with the period of 100~120s for single nanochannel.

16. Standard fluid-kinetics notation

$$\nabla P = \frac{8\mu l Q}{\pi R^4}$$

Where:

∇P is the pressure difference between the two ends

L is the length of channel

μ is the dynamic viscosity

R is the pore radius.

As we know, the pore radius is extremely tiny in single conical nanochannel which the maximum (base side) is *ca.* 750 nm. Consequently, the reciprocal of its fourth power is colossal, directly resulting in ultrahigh flow resistance, estimating up to Gpa.

17. Multiple deliberate operations

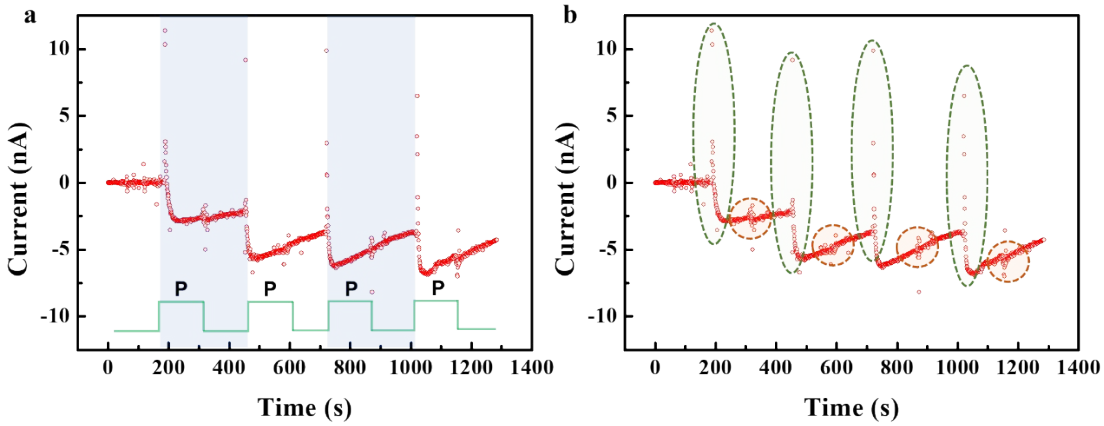

Figure S15 Detailed illustration of multiple operations. (a) the hot electrolyte was immersed into the system and then removed. (b) the green circle emphasized that the positive current always appeared and then it decreased to negative values, which implied that the transmit speed of pressure were faster than that of temperature and the influence of temperature gradient outplayed its rival in the contest in the short while. The brown circle emphasized that variance ratio of current varied before and after removing the external pressure on each process due to dissipation speed of heat depending on the volume of bulk phase.

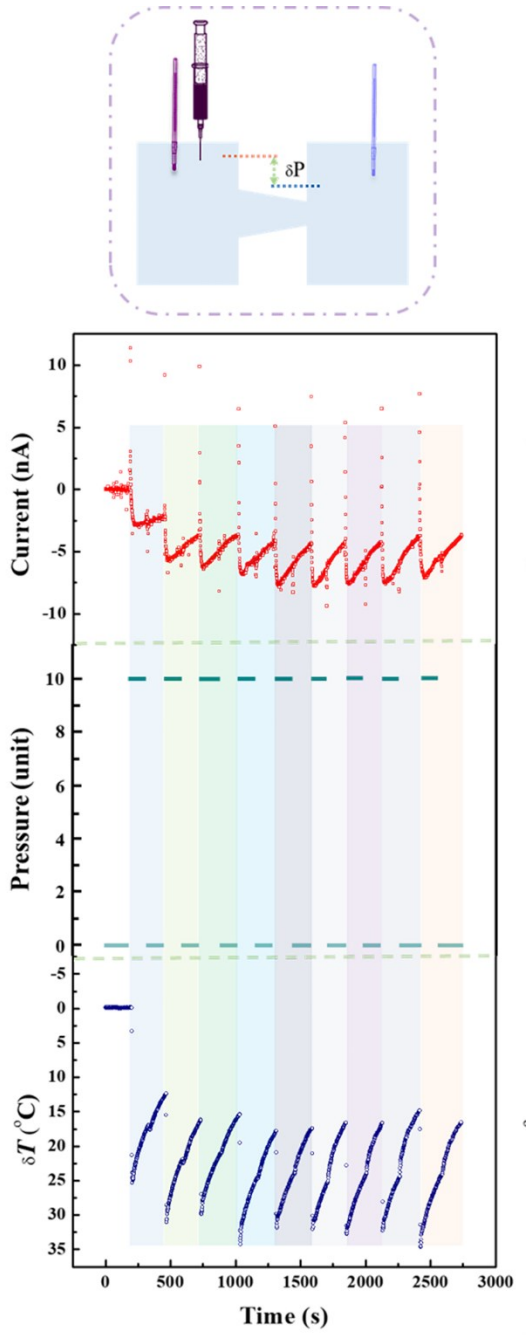

Figure S16 Multiple deliberate operations until the temperature difference changed intermittently.

18. Multiple deliberate operations

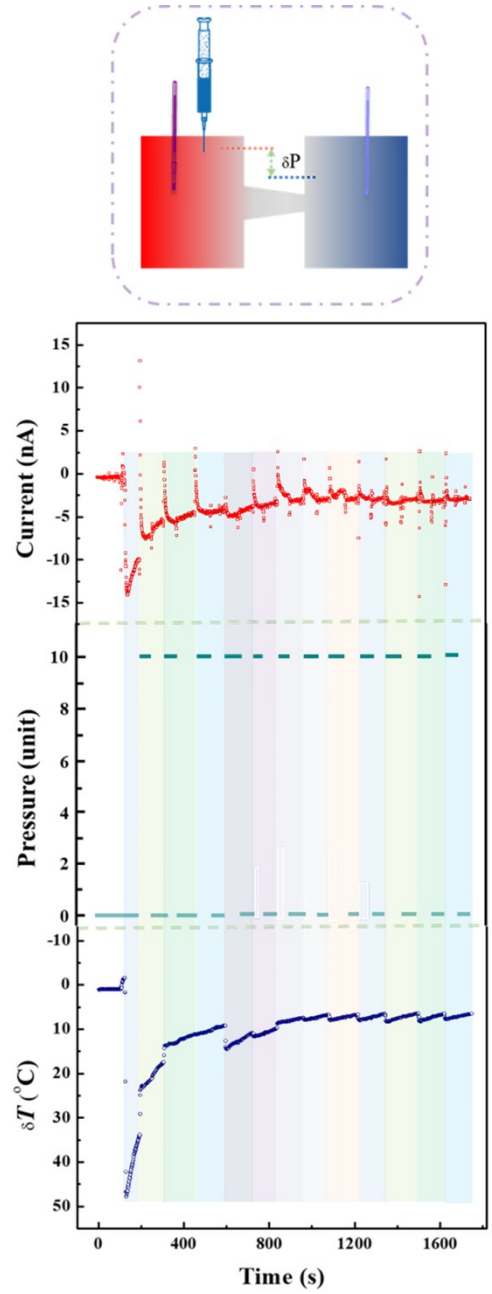

Figure S17 3 nA was obtained at the temperature gradient of 7 ℃ under confrontational pressure gradient.

1. Miansari, M.; Friend, J. R., Acoustic Nanofluidics via Room Temperature Lithium Niobate Bonding: A Platform for Actuation and Manipulation of Nanoconfined Fluids and Particles. *Adv. Funct. Mater.* **2016,** *26* (43), 7861-7872.
2. Tivony, R.; Safran, S.; Pincus, P.; Silbert, G.; Klein, J., Charging dynamics of an individual nanopore. *Nat. commun.* **2018,** *9* (1), 4203.
3. Dietzel, M.; Hardt, S., Thermoelectricity in Confined Liquid Electrolytes. *Phys. Rev. Lett.* **2016,** *116* (22), 225901.
4. Vlassiouk, I.; Smirnov, S.; Siwy, Z., Ionic Selectivity of Single Nanochannels. *Nano Lett.* **2008,** *8* (7), 1978-1985.
5. Vlassiouk, I.; Smirnov, S.; Siwy, Z., Nanofluidic Ionic Diodes. Comparison of Analytical and Numerical Solutions. *Acs Nano* **2008,** *2* (8), 1589-1602.
6. Bocquet, L.; Charlaix, E., Nanofluidics, from bulk to interfaces. *Chem. Soc. Rev.* **2010,** *39* (3), 1073-1095.
7. Petsev, D. N.; Lopez, G. P., Electrostatic Potential and Electroosmotic Flow in a Cylindrical Capillary filled with Symmetric Electrolyte: Analytic Solutions in Thin Double Layer Approximation. *J. Colloid Inter. Sci.* **2006,** *294* (2), 492-498.
8. Xie, G.; Li, P.; Zhang, Z.; Xiao, K.; Kong, X.; Wen, L.; Jiang, L., Skin-Inspired Low-Grade Heat Energy Harvesting Using Directed Ionic Flow through Conical Nanochannels. *Adv. Energy Mater.* **2018,** *8* (22), 1800459.
9. Chen, K.; Yao, L.; Su, B., Bionic Thermoelectric Response with Nanochannels. *J. Am. Chem. Soc.* **2019,** *141* (21), 8608-8615.
10. Wu, J.; Black, J. J.; Aldous, L., Thermoelectrochemistry using conventional and novel gelled electrolytes in heat-to-current thermocells. *Electrochimica Acta* **2017,** *225*, 482-492.
11. Yang, P.; Liu, K.; Chen, Q.; Mo, X.; Zhou, Y.; Li, S.; Feng, G.; Zhou, J., Wearable Thermocells Based on Gel Electrolytes for the Utilization of Body Heat. *Angew. Chem. Int. Edit.* **2016,** *55* (39), 12050-12053.
12. Pu, S.; Liao, Y.; Chen, K.; Fu, J.; Zhang, S.; Ge, L.; Conta, G.; Bouzarif, S.; Cheng, T.; Hu, X.; Liu, K.; Chen, J., Thermogalvanic Hydrogel for Synchronous Evaporative Cooling and Low-Grade Heat Energy Harvesting. *Nano Lett.* **2020,** *20* (5), 3791-3797.